JOURNAL OF PROPULSION AND POWER
Vol. 21, No. 3, May–June 2005

Numerical and Experimental Studies of Injection Modeling for Supersonic Flame-Holding

Sadegh Tabejamaat*
Amirkabir University of Technology, 15875-4413 Tehran, Iran
and
Hideaki Kobayashi† and Takashi Niioka†
Tohoku University, Sendai 980-77, Japan

The effects of injection modeling on the combustion of hydrogen in a supersonic airflow are considered here using both numerical and experimental approaches. Two types of injection, single and double from the base of a strut, are analyzed in depth. The solutions to the governing equations of the numerical simulation including Navier–Stokes (N–S) equations, turbulence model, and finite full chemistry are brought in using a high-order numerical scheme. In particular, the laser-induced-fluorescence (LIF) method is effectively used for the OH radical recording. The flame structures of two different injection models are simulated separately using both numerical and experimental techniques for comparison. As a result of changes in the flowfield as well as mixing phenomenon, the flame structure of the double-slit injection model is significantly different from the one for the single injection. By increasing the slit interval of the double-slit injection, the model can face the blowout when $d > 8$ mm. Furthermore, an increase in the slit width can also affect the flowfield of the wake significantly so that the combustion zone will expand downstream.

Introduction

IN general, the combustor of a scramjet (supersonic combustion ramjet) requires an efficient flame-holding method. The residence time of the airflow in a scramjet engine is usually quite short of the order of a millisecond. During this short time, the fuel and air are mixed, resulting in burning and then stabilizing state to achieve maximum thrust.[1,2]

Several vital experiments as well as theoretical and numerical studies have been conducted already in the field of supersonic combustion in the past two decades.[3] It seems between all of those that the injection method has a vitally important role in the flame-holding development. As it appears from the amount of published work, the flame-holding techniques such as parallel injection, transverse injection, plasma injection, and shock-wave-induced method have been studied broadly in the past.[4]

In particular, the parallel injection through a base of strut is considered as an efficient approach for flame-holding, in which the contact area between the streams of fuel and air increases significantly, resulting a better enhancement in the mixing and reaction rates.

The main principles of parallel injection in subsonic flow and flame stabilization using recirculation zones are well presented by Zukoski and Marble.[5] By assuming some approximations in the subsonic flame stabilization, they concluded that the residence time is directly proportional to the length of the recirculation zone and inversely proportional to the amount of the velocity. Therefore, the residence time strongly depends on the geometrical size of the recirculation zone. As a result, it is suggested that a similar principle can be used for the stabilization of supersonic combustion.[6] On the other hand, generating a zone of recirculation can provide a region of enhanced mixing (i.e., fluid-dynamic concept) as well as a region of radical development resulting an intense combustion zone in turn.

Received 15 February 2004; revision received 17 August 2004; accepted for publication 10 September 2004.

*Assistant Professor, Department of Aerospace Engineering, Hafez Avenue, P.O. Box 15875-4413; stabe@aut.ac.ir.
†Professor, Institute of Fluid Science.

At the present study, the fuel injection from the base of a strut is applied as a physical model to study the effect of injection modeling on combustion in supersonic airflow. Some numerical simulations and experiment work have been comprehensively conducted on two different models using the single-slit and double-slit injections.

First of all, the dimensional effects of the flame-holder and nozzle size on the flame holding are studied in detail. Then, the required numerical calculations and experiments are described for the injection of hydrogen from both single- and double-slit patterns. At last, various effects of slit interval and slit width on flame-holding regime and flame structure are considered.

Governing Equations and Numerical Scheme

The nondimensional Navier–Stokes equations in the generalized curvilinear coordinates (ξ, η, ζ) for a time-dependent, multidimensional, chemically reacting flow with n species and finite-rate chemistry can be written as

$$\frac{\partial \boldsymbol{U}}{\partial \boldsymbol{t}} + \frac{\partial (\boldsymbol{F} - \boldsymbol{F}_v)}{\partial \xi} + \frac{\partial (\boldsymbol{G} - \boldsymbol{G}_v)}{\partial \eta} = \boldsymbol{S} \tag{1}$$

where

$$\boldsymbol{U} = \boldsymbol{J}\tilde{\boldsymbol{U}}, \qquad \boldsymbol{F} = \boldsymbol{J}(\xi_x \tilde{\boldsymbol{F}} + \xi_y \tilde{\boldsymbol{G}})$$

$$\boldsymbol{G} = \boldsymbol{J}(\eta_x \tilde{\boldsymbol{F}} + \eta_y \tilde{\boldsymbol{G}}), \qquad \boldsymbol{F}_v = \frac{\boldsymbol{J}}{\boldsymbol{Re}_0}(\xi_x \tilde{\boldsymbol{F}} + \xi_y \tilde{\boldsymbol{G}})$$

$$\boldsymbol{G}_v = \frac{\boldsymbol{J}}{\boldsymbol{Re}_0}(\eta_x \tilde{\boldsymbol{F}} + \eta_y \tilde{\boldsymbol{G}}), \qquad \boldsymbol{S} = \frac{\boldsymbol{J}}{\boldsymbol{Da}_0}\tilde{\boldsymbol{S}}$$

$$\boldsymbol{J} = \frac{\partial(\boldsymbol{x}, \boldsymbol{y})}{\partial(\xi, \eta)} = \boldsymbol{x}_\xi \boldsymbol{y}_\eta - \boldsymbol{x}_\eta \boldsymbol{y}_\xi \tag{2}$$

In the preceding relations, $\boldsymbol{J}$ is the Jacobian of coordinate transformation, and $\boldsymbol{Re}_0$ and $\boldsymbol{Da}_0$ are the Reynolds and Damkohler numbers based on the reference parameters, respectively. The parameter $\tilde{\boldsymbol{U}}$ is the vector of conservation variables; $\tilde{\boldsymbol{F}}$ and $\tilde{\boldsymbol{G}}$ are the vectors of convective fluxes; $\tilde{\boldsymbol{F}}_v$ and $\tilde{\boldsymbol{G}}_v$ are their viscous components; and $\tilde{\boldsymbol{S}}$ is a vector of source term. In a conservative form, these vectors can

be presented as

$$\tilde{\boldsymbol{U}} = \begin{bmatrix} \rho_i \\ \rho \boldsymbol{u} \\ \rho \boldsymbol{v} \\ \boldsymbol{E} \end{bmatrix}, \qquad \tilde{\boldsymbol{F}} = \begin{bmatrix} \rho_i \boldsymbol{u} \\ \rho \boldsymbol{u}^2 + \boldsymbol{p} \\ \rho \boldsymbol{v} \\ (\boldsymbol{E} + \boldsymbol{p})\boldsymbol{u} \end{bmatrix}$$

$$\tilde{\boldsymbol{G}} = \begin{bmatrix} \rho_i \boldsymbol{v} \\ \rho \boldsymbol{u} \\ \rho \boldsymbol{v}^2 + \boldsymbol{p} \\ (\boldsymbol{E} + \boldsymbol{p})\boldsymbol{v} \end{bmatrix}, \qquad i = 1, n$$

$$\tilde{\boldsymbol{F}}_v = \begin{bmatrix} -\rho_i \boldsymbol{u}_i \\ T_{xx} \\ T_{xy} \\ \boldsymbol{u}T_{xx} + \boldsymbol{v}T_{xy} - \boldsymbol{q}_x \end{bmatrix}, \qquad \tilde{\boldsymbol{G}}_v = \begin{bmatrix} -\rho_i \boldsymbol{v}_i \\ T_{xy} \\ T_{yy} \\ \boldsymbol{u}T_{xy} + \boldsymbol{v}T_{yy} - \boldsymbol{q}_y \end{bmatrix}$$

$$\tilde{\boldsymbol{S}} = \begin{bmatrix} \dot{\omega}_i \\ 0 \\ 0 \\ 0 \end{bmatrix} \tag{3}$$

where ρ_i, ρ, $\boldsymbol{u}$, $\boldsymbol{v}$, $\boldsymbol{p}$, and E are the species density, the density, the x and y components of velocity, the static pressure, and the total energy, respectively. As introduced before, instead of solving the total density and $n-1$ species equations, the scheme in this paper can solve n-species equations in a fully coupled manner. As a result, the concentrated computational error on the nth species can be avoided. Assuming that the ideal-gas equation can be applied for any species, the static pressure can be calculated from the following equation:

$$\boldsymbol{p} = \rho \boldsymbol{T} \sum_{i=1}^{n} \boldsymbol{R}_i \boldsymbol{Y}_i \tag{4}$$

where T is temperature and $\boldsymbol{R}_i$ and $\boldsymbol{Y}_i$ are the gas constant and mass fraction of the species I, respectively. Therefore, the total energy can be written as

$$\boldsymbol{E} = \boldsymbol{T} \sum_{i=1}^{n} \rho \boldsymbol{h}_i \boldsymbol{Y}_i - \boldsymbol{p} + \frac{1}{2}\rho(\boldsymbol{u}^2 + \boldsymbol{v}^2) + \rho \boldsymbol{q}^2 \tag{5}$$

The enthalpy of species in this equation can be calculated from

$$\boldsymbol{h}_i = \boldsymbol{h}_i^0 + \int_{T_{\text{ref}}}^{T} \boldsymbol{C}_{\text{pi}}\, \mathrm{d}\boldsymbol{T} \tag{6}$$

The shear and normal stresses and the energy fluxes caused by conduction and species diffusion are expressed as

$$T_{xx} = 2(\mu + \mu_t)\frac{\partial \boldsymbol{u}}{\partial \boldsymbol{x}} - \frac{2}{3}(\mu + \mu_t)\left(\frac{\partial \boldsymbol{u}}{\partial \boldsymbol{x}} + \frac{\partial \boldsymbol{v}}{\partial \boldsymbol{y}}\right) - \frac{2}{3}\rho \boldsymbol{k}$$

$$T_{yy} = 2(\mu + \mu_t)\frac{\partial \boldsymbol{v}}{\partial \boldsymbol{y}} - \frac{2}{3}(\mu + \mu_t)\left(\frac{\partial \boldsymbol{u}}{\partial \boldsymbol{x}} + \frac{\partial \boldsymbol{v}}{\partial \boldsymbol{y}}\right) - \frac{2}{3}\rho \boldsymbol{k}$$

$$\boldsymbol{q}_y = -\boldsymbol{C}_p\left(\frac{\mu}{\boldsymbol{P}_r} + \frac{\mu_t}{\boldsymbol{P}_{r_t}}\right)\frac{\partial \boldsymbol{T}}{\partial \boldsymbol{y}} + \left(\mu + \frac{\mu_t}{\sigma_k}\right)\frac{\partial \boldsymbol{k}}{\partial \boldsymbol{y}} + \rho \sum_{i=1}^{n} \boldsymbol{D}_i \boldsymbol{h}_i \frac{\partial \boldsymbol{Y}_i}{\partial \boldsymbol{y}} \tag{7}$$

The heat of formation and specific heat of species are taken from JANNAF.[7] The specific heat of $\boldsymbol{i}$ species $\boldsymbol{C}_{\text{pi}}$ is calculated from a fourth-order polynomial equation in terms of the variable of temperature. This equation is the result of curve fitting using the data given in the JANNAF. To solve the series of polynomial equations, it is required that the corresponding coefficients are determined here for each species. Similar to the procedure used in JANNAF, $\boldsymbol{T}_{\text{ref}}$ is assumed as 298.15 K;

$$C_{\text{pi}} = \boldsymbol{a}_{0i} + \boldsymbol{a}_{1i}\boldsymbol{T} + \boldsymbol{a}_{2i}\boldsymbol{T}^2 + \boldsymbol{a}_{3i}\boldsymbol{T}^3 + \boldsymbol{a}_{4i}\boldsymbol{T}^4 \tag{8}$$

In general, the thermal conductivity λ, the coefficient of viscosity μ, and the diffusion coefficient $\boldsymbol{D}_i$ are mainly obtained from the kinetic theory of gases. In the process of molecular transport, the deviation from the ideal model of rigid elastic spheres (i.e., known as real-gas behavior) should be taken into consideration. Accordingly, the transfer energy between internal degree of freedom and the translational motion for a polyatomic gas, an appropriate relation, are introduced here for the practical purposes (also, see Ref. 8):

$$\lambda_i = 8.323 \times 10^{-3}\left(\sqrt{T/M_i}\Big/\sigma_i^2 \Omega_i^{(2.2)}\right) + 1.32(\mu_i/M_i)(C_{\text{pi}} - 2.5R_i) \tag{9}$$

where σ_i and $\Omega_i^{(2.2)}$ are the low-velocity collision diameter and the reduced collision integral of species, respectively. The parameter $\Omega_i^{(2.2)}$ is a unique function of the reduced temperature, which represents the ratio of the absolute temperature and the depth of the intermolecular potential. The thermal conductivity of a gas mixture can be estimated from λ_i and the mole fraction of the pure species $\boldsymbol{x}_k$ using the following empirical relation[9]:

$$\lambda = \sum_{i=1}^{n}\left[\lambda_i \Big/ \left(1 + \sum_{R=i} x_k \cdot 1.065\varphi_{\text{ik}}\right)\right] \tag{10}$$

The correction factor ϕ_{ik} mainly depends on the viscosity coefficient μ_i and the molar masses M_i of the species i, and it is calculated from

$$\varphi_{\text{ik}} = \frac{1}{2\sqrt{2}}\left(1 + \frac{M_i}{M_k}\right)^{-\frac{1}{2}}\left[1 + \left(\frac{\mu_i}{\mu_k}\right)^{\frac{1}{2}} \cdot \left(\frac{M_i}{M_k}\right)^{\frac{1}{4}}\right]^2, \qquad \left[\frac{\text{Kg}}{\text{m.s}}\right] \tag{11}$$

The viscosity coefficient of species i is determined from[10]

$$\mu_i = 2.6693 \cdot 10^{-6}\frac{\sqrt{\boldsymbol{M}_i \boldsymbol{T}}}{\sigma_i^2 \cdot \Omega_i^{(2.2)}} \tag{12}$$

where M_i is in grams/mole T is in degrees Kelvin and σ_i is in nanometers. Wilke[11] suggested the following empirical equation when a mixture of gases is used, similar to the thermal conductivity:

$$\mu = \sum_{i=1}^{n}\left[\mu_i \Big/ \left(1 + \sum_{k \neq i} \frac{x_k}{x_i}\varphi_{\text{ik}}\right)\right] \tag{13}$$

where ϕ_{ik} is determined using Eq. (11).

For the mass transport by concentration gradient, Fick's law states that the mass flux is primarily proportional to the concentration gradient as follows:

$$\rho_i \boldsymbol{u}_i = -\rho \boldsymbol{D}_i \frac{\partial \boldsymbol{Y}_i}{\partial \boldsymbol{x}}, \qquad \rho_i \boldsymbol{v}_i = -\rho \boldsymbol{D}_i \frac{\partial \boldsymbol{Y}_i}{\partial \boldsymbol{y}} \tag{14}$$

In this case, the binary diffusion coefficient is estimated by the following equation[8]:

$$\boldsymbol{D}_{\text{ik}} = 0.185 \times 10^{-6}\frac{\boldsymbol{T}^{\frac{3}{2}}\sqrt{\boldsymbol{M}_i + \boldsymbol{M}_k}}{\boldsymbol{P}_{\text{atm}}\sigma_{\text{ik}}^2 \Omega_{\text{D,ik}}\sqrt{\boldsymbol{M}_i \boldsymbol{M}_k}} \tag{15}$$

where the collision integral $\Omega_{\text{d,ik}}$ is

$$\Omega_{\text{D,ik}} = \boldsymbol{T}_{\text{ik}}^{*\,-0.145} + \left(\boldsymbol{T}_{\text{ik}}^{*} + 0.5\right)^{-2.0} \tag{16}$$

and

$$\sigma_{\text{ik}} = (\sigma_i + \sigma_k)/2, \qquad \boldsymbol{T}_{\text{ik}}^{*} = \sqrt{\boldsymbol{T}_i^{*}\boldsymbol{T}_i^{*}} \tag{17}$$

The parameter T_i^* is the reduced temperature. For a mixture, the empirical law is implemented as[12]

$$D_i = \frac{1 - Y_i}{\sum_{j \neq i}(x_i / D_{ik})} \tag{18}$$

where Y_i and x_i indicate the mass fraction and the mole fraction of the species i, respectively.

Turbulence Model

When the supersonic combustion is considered, there will be some vital interactions between turbulence, shock wave, and chemistry that require further investigation compared to other types of combustion. The existing pdf models, which largely account for the interaction between turbulence and chemistry, are usually based on the fast chemistry assumption, flamelet conception, or the multivariable pdf approximation.[13] When the effects of finite-rate chemistry, shocklets, and differential diffusion become significant, the applicability of these pdf models to supersonic combustion can still remain a problematic task.[14,15] However, taking all of these effects into consideration requires a sophisticated moment-closure turbulence model, which is out of the research direction in this paper, and it is discussed further here.

The total stress tensor T_{ij} and the heat-flux vector q_j in the Reynolds-averaged Navier–Stokes equation can be expressed other way around using the concepts of turbulent eddy viscosity μ_t and the Boussinesq approximation. The low-Reynolds-number q-ε turbulence model of Coakley and Huang[16] in the Navier–Stokes equations satisfactorily is powerful enough to predict the behavior of the supersonic flow as reported by Coakley and Huang[16] and Gerlinger et al.[17] In this case, the turbulent eddy viscosity μ_t is modeled as

$$\mu_t = C_\mu f_\mu \rho(k^2/\varepsilon) = C_\mu f_\mu \rho q l$$

$$q = \sqrt{k}, \qquad \varepsilon = \omega k, \qquad l = q^3/\varepsilon \tag{19}$$

where the variables in these equations are k, the turbulent kinetic energy; ε, the dissipation of turbulent velocity scale; l, the length scale; and ω, the specific dissipation rate or frequency scale. In addition, C_μ is the constant of the model, and f_μ is the model-damping function, which both improve the model prediction at the vicinity of the wall effects or in a low-Reynolds-number region. The variables of q and ω can be calculated from the following partial differential equations:

$$\frac{\partial U_{q\omega}}{\partial t} + \frac{\partial (F_{q\omega} - F_{q\omega_v})}{\partial x} + \frac{\partial (G_{q\omega} - G_{q\omega_v})}{\partial y} = S_{q\omega} \tag{20}$$

where

$$U_{q\omega} = \begin{bmatrix} \rho q \\ \rho \omega \end{bmatrix}, \qquad F_{q\omega} = \begin{bmatrix} \rho u q \\ \rho u \omega \end{bmatrix}, \qquad G_{q\omega} = \begin{bmatrix} \rho v q \\ \rho v \omega \end{bmatrix}$$

$$F_{q\omega_v} = \begin{bmatrix} \left(\mu + \dfrac{\mu_t}{\sigma_q}\right)\dfrac{\partial q}{\partial x} \\ \left(\mu + \dfrac{\mu_t}{\sigma_\omega}\right)\dfrac{\partial \omega}{\partial x} \end{bmatrix}, \qquad G_{q\omega_v} = \begin{bmatrix} \left(\mu + \dfrac{\mu_t}{\sigma_q}\right)\dfrac{\partial q}{\partial y} \\ \left(\mu + \dfrac{\mu_t}{\sigma_\omega}\right)\dfrac{\partial \omega}{\partial y} \end{bmatrix}$$

$$S_{q\omega} = \begin{bmatrix} \left[C_{q1} C_\mu f_1 \left(\dfrac{s}{\omega}\right)^2 - \alpha_1 \dfrac{D}{\omega} - C_{q2} \right] \rho \omega q \\ \left[C_{\omega_1} C_\mu f_2 \left(\dfrac{s}{\omega}\right)^2 - \alpha_2 \dfrac{D}{\omega} - C_{\omega_2} \right] \rho \omega^2 \end{bmatrix}$$

$$S^2 = 2\left[\left(\frac{\partial u}{\partial x}\right)^2 + \left(\frac{\partial v}{\partial y}\right)^2\right] + \left(\frac{\partial u}{\partial y} + \frac{\partial v}{\partial x}\right)^2 - \frac{2}{3}\left(\frac{\partial u}{\partial x} + \frac{\partial v}{\partial y}\right)^2 \tag{21}$$

Coakley suggests the following initial values for the constants and functions of the model to be used in the estimation process:

$$C_\mu = 0.09, \qquad C_{\omega_1} = 0.555, \qquad \sigma_q = 0.8$$

$$C_{q1} = C_{q2} = 0.5, \qquad C_{\omega_2} = 0.833, \qquad \sigma_\omega = 2.0$$

$$\alpha_1 = \tfrac{2}{3} C_{q1} = 0.333, \qquad \alpha_2 = \tfrac{2}{3} C_{\omega_1} = 0.37$$

$$f_1 = f_\mu, \qquad f_2 = 1 \tag{22}$$

Near to the wall or in a low-Reynolds region,

$$f_\mu = 1 - \exp(-0.022 R_q)$$

$$R_q = qy/v, \qquad C_{\omega_1} = 0.055 + 0.5 f_\mu \tag{23}$$

Chemistry Model

In this research work, the finite-rate full-mechanism chemistry model has been widely used. It is well known that the constant of the specific reaction rate is usually evaluated by the Arrhenius law as follows:

$$K_{f,k}, K_{b,k} = B_k T^{N_k} \exp[-(E_k / R^\circ T)] \tag{24}$$

where the frequency factors B_k and N_k and the activation energy E_k are specified for any reaction. In general, a reaction mechanism for the multistep reversible reaction can be written as

$$\sum_{i=1}^{NS} v'_{ji} C_i \leftrightarrow \sum_{i=1}^{NS} v''_{ji} C_i \tag{25}$$

The net rate of change in mole concentration of species i by reaction j is

$$C_{ij} = \left(\sum_{k=1}^{NS} \alpha_{kj} C_k\right)^\beta (v''_{ji} - v'_{ji}) \left(k_{f,j} \prod_{k=1}^{NS} C_k^{v'_{ji}} - k_{b,k} \prod_{k=1}^{NS} C_k^{v''_{ji}}\right) \tag{26}$$

where v_{ji} is the stoichiometric coefficient of species i for the reaction steps j, with the single prime and double prime, which represent the reactant and the product, respectively. Parameter $\beta = 1$ is the three-body reaction, and α is the third-body efficiency. The overall production of species i is

$$\dot{\omega}_i = W_i \sum_{j=1}^{NR} \dot{C}_{ij} \tag{27}$$

where W_i is the molecular weight.

In this research work, the full chemistry mechanism developed by Stahl and Warnatz[18] is used. This mechanism considers nine species (H_2, O_2, H_2O, OH, H, O, HO_2, H_2O_2, and N_2) with 37 reactions in total.

Numerical Scheme

The lower-upper symmetric successive overrelaxation (LU-SSOR) scheme was originally developed by Shuen and Yoon.[19] This scheme has relatively higher computational efficiency and stability than the alternating direction implicit scheme in general and for multidimensional problem in particular. In the current study, the transient part of governing equations is thoroughly solved using LU-SSOR scheme.

Based on the total-variation-diminishing (TVD) conditions, several TVD schemes have been generated so far and successfully applied to the shock capturing and strongly discontinuous surface waves. In this paper, the convection term of governing equation is calculated using a TVD MUSCL approach.[20]

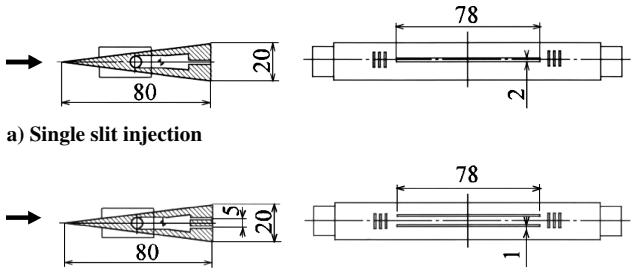

a) Single slit injection

b) Double slit injection

Fig. 1 Sketch of physical model.

Numerical and Experimental Modelings

Figure 1 shows a sketch of experimental model of the strut used in this research work. For the numerical studies, the model is set as a two-dimensional strut with the fuel injection from the base of the strut.

The results of two types of single-slit and double-slit injection models are given in this paper. For the whole computational domain, an H-type grid system with totally 221×131 points is used. To achieve a high resolution in the wake region, sufficient grids should be utilized in both jet and shear-layer regions. A grid-resolution study has been conducted in order to verify the grid independence of the results. To ensure the results' convergence, the variations and fluctuations of main parameters such as velocity, pressure, temperature, and species mole fraction have been monitored carefully during the entire calculation process.

There are some separate nitrogen injection slits on both sides of the fuel slit of the experimental model to eliminate the lateral-eddy region and practically to maintain the two-dimensional fuel injection. The inflow of the model is a two-dimensional supersonic airflow with the specification of $M_{\text{air}} = 2.5$, $P_{\text{air}} = 0.05$ MPa, and $T_{\text{air}} = 298$ K. The sonic cold hydrogen fuel with the temperature of 298 K is injected into the model using the nozzles. A rich fuel preburning in the strut has been used for the ignition. The flow rates of hydrogen and air were separately controlled by a combination of different orifices and solenoid valves to provide the flow rate required. To prevent a flame backlash, the mixture is going through a one-way pipe right away before reaching into the preburner. The experiment was conducted at relatively a wide range of hydrogen flow rate of $Q_{\text{H2}} = 50 \sim 1000$ Nl/min. The strut was placed at the test section of a blowdown supersonic wind tunnel, where the nozzle exit diameter is 135 mm. Practically, each test has been done within 20 s, while the total pressure and temperature were within 0.45–0.5 MPa and 450–850 K, respectively. The main airflow Mach number was kept constant at 2.5 throughout the test.

Results and Discussion

Flame Holding in Supersonic Airflow

In this research, a self-ignition of a hydrogen/air mixture is obtained using a preburner. In the preburner, hydrogen burns with air and is injected into the supersonic airflow. In the current numerical simulation, the minimization technique used in the Gibss' free-energy approach to a chemical equilibrium is applied to maintain the equilibrium state in the preburner.[21]

The validation of numerical code has already been reported in detail by the author in Ref. 22. Some further validations can be found in the report when the numerical and experimental results of the fuel injection are discussed. Figure 2 is used to compare the outcomes of the experiment and numerical simulations, and it shows the experimental direct photograph and numerical temperature distribution of the flame at the wake flow of the model shown in Fig. 1. For the data presented in Fig. 2, the Mach number, the airflow temperature, and pressure are 2.5, 293 K, and 0.05 MPa, respectively. As can be seen in Fig. 2, the flame structures of both aforementioned cases consist of a primary combustion region near the base and a substantial combustion region in the downstream. It will be shown that the OH recording also indicates the same structure.

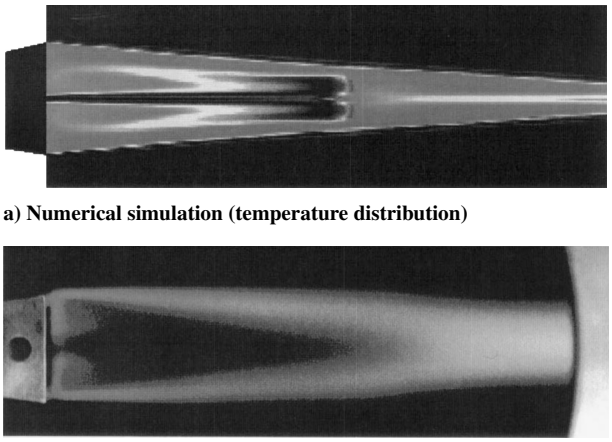

a) Numerical simulation (temperature distribution)

b) Experiment (direct photograph)

Fig. 2 Comparison of flame direct photograph and numerical temperature distribution.

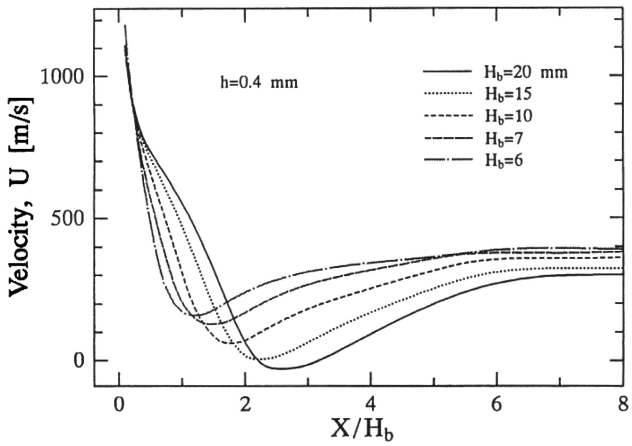

Fig. 3 Variation of axial velocity at centerline along X.

Mixing Efficiency

Mixing between air and fuel has a paramount importance in supersonic combustion. To obtain a quantitative feature of mixing, the mixing efficiency is defined as

$$M_{\text{eff}} = \int_0^H \frac{4\phi}{(1+\phi)^2} \frac{\mathrm{d}y}{H} \tag{28}$$

where ϕ and H are the equivalence ratio and the lateral space of the computational domain, respectively. The mixing efficiency takes a maximum value of one at stoichiometry and zero when either hydrogen or oxidizer mole fraction is vanished.

Strut and Nozzle Modeling

The scales of the injection port shown in Fig. 1 can be altered in two different ways. One approach is that the width of the strut base H_b is changed to consider the effects of the recirculation zone on the flame holding. The second approach is that the nozzle-exit size is enlarged so that the effects of the fuel mass flow rate on the flame stability are studied.

By having the experience in the subsonic flame-holding, it is now necessary to know how the sizing scale of the model affects the combustion process. On the other hand, as each scale can provide a particular recirculation zone it is important to examine whether the aforementioned relationship between the recirculation length and the flame holding in the subsonic flow is technically valid for the combustion process in the supersonic flow as well.

The variation of axial velocity at the centerline along X axis is shown in Fig. 3 for various H_b. In this setup, $H_b = 15$ mm is used as the axial distance. The velocity profiles in this figure generally show

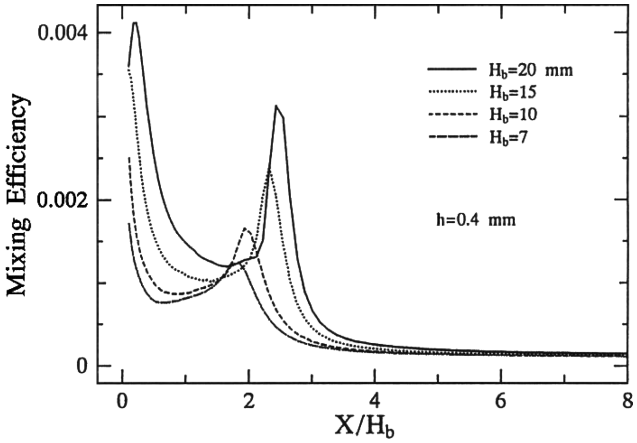

Fig. 4 Variations of mixing efficiency along X.

a high velocity region near the base because of the vicinity of the injection when the injection velocity at nozzle exit is about 1022 m/s. The flow regime is decelerated by the viscosity of the shear layer at first, and then, it is accelerated again in the redeveloped zone downstream. The experimental results (see Ref. 23) related to the base flow without any injection show that the impingement of the shear layers likely occurs at $X/H_b = 1.37$. After considering the effects of both injection and combustion phenomena on the expansion process of the recirculation region, it is concluded that the impingement point moves downstream. There is a strong reverse flow in the recirculation zone at $H_b = 20$ mm with comparably a long recirculation region. As H_b decreases, the reverse flow region becomes smaller so that the reverse flow region tends to be very small at $H_b < 6$ mm.

The variation of the mixing efficiency for different H_b along the X axis is shown in Fig. 4. It can be seen that the change of mixing efficiency provides two maximum points: near the base and just around the impinging point. The first one is mainly caused by large-scale vortices near the base, particularly in the corners that face high mixing efficiency. The second maximum point corresponds to another large-scale vortex in the trailing region of the recirculation zone. The diffusion of the fuel into the airflow occurs somewhere between these two points in a narrow region of the mixing layer. Therefore, a strong turbulent region is restricted to a narrow area of shear layer in this transition.

The consideration of the mixing efficiency curve along with the velocity profile (shown in Fig. 3) shows that the region of high mixing efficiency apparently remains inside the recirculation region. In addition, Fig. 4 shows that the efficiency of the second strong mixing region considerably reduces when H_b decreases. This concept is important in the development of the combustion downstream. The distribution patterns of OH mole fraction are shown in Fig. 5 in order to have a two-dimensional feature of the combustion development. Through this research work, it is realized that those reactions involving the OH production are relatively slow and dominating the combustion. Therefore, in the combustion of hydrogen OH is a very important radical, and its distribution can demonstrate combustion development. Clearly, Fig. 5 demonstrates the combustion region laterally becoming smaller when H_b decreases. At $H_b = 20$ mm, a large recirculation region enables good mixing between the hydrogen and air. One of the most important characteristics of such a large recirculation zone is the enhancement of the mixing throughout the recirculation zone. In particular, the focus would be on the expansion of the mixing phenomenon between two strong combustion regions shown in Fig. 4. On the other hand, there are two strong combustion regions created by two strong mixing zones as shown in Fig. 4.

In general, it seems the expansion of the combustion region downstream would be very important to the flame holding. Otherwise, the flame would be limited to a small region near the base. As a result, the development of the substantial combustion region strongly depends on the growth of combustion following the primary combustion

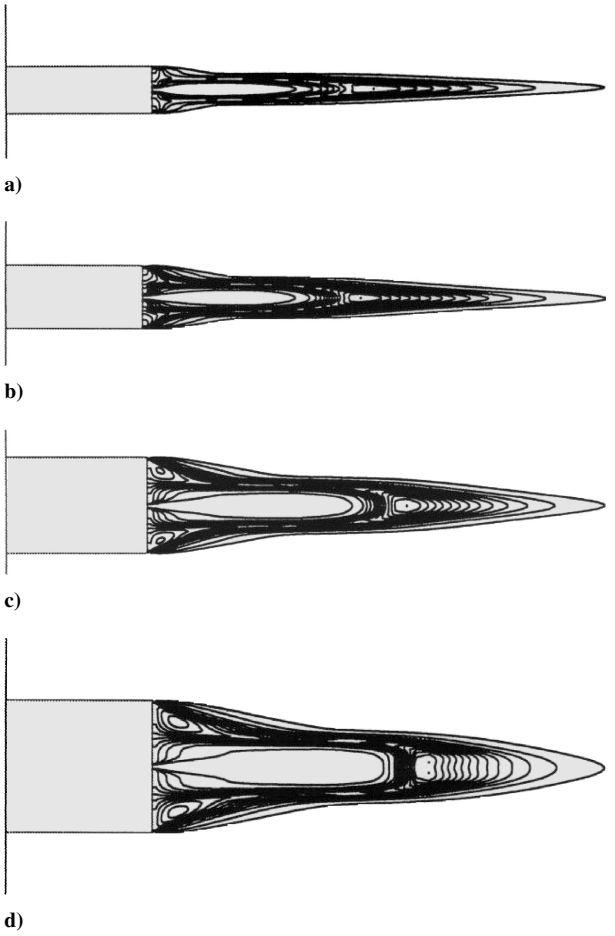

Fig. 5 Distributions of OH mole fraction: a) $H_b = 7$ mm, b) $H_b = 10$ mm, c) $H_b = 15$ mm, and d) $H_b = 20$ mm.

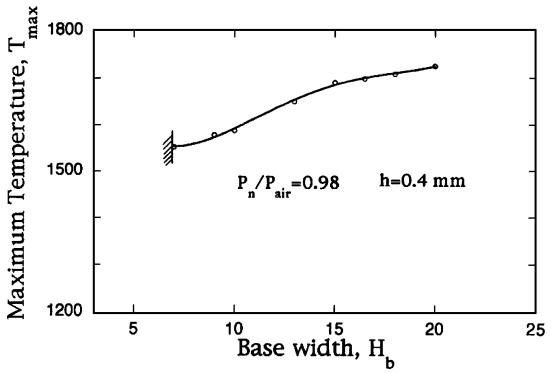

Fig. 6 Variation of maximum temperature in combustion region against the base width H_b.

region. Therefore, a significant conclusion from Fig. 5 is that the combustion in this transition region and the substantial combustion are both enhanced for larger H_b. This means the flame holding strongly depends on the length of recirculation zone. In the case of $H_b < 7$ mm, it seems the combustion region cannot be established at all. This conclusion has been made carefully following several determinations using $4 \leq H_b \leq 10$ mm.

Figure 6 shows how the maximum temperature inside the combustion region varies in terms of H_b. As soon as the base width increases, the maximum temperature starts to rise, and accordingly for smaller H_b the recirculation zone becomes drastically small resulting an extinction at $H_b < 7$ mm.

The scale of the nozzle exit is set in the same way as the base scale affecting the establishment of the mixing region. The mesh

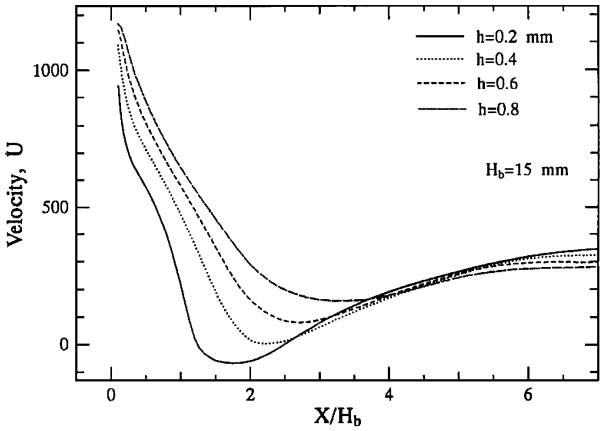

Fig. 7 Variation of axial velocity at centerline along X against nozzle exit size h.

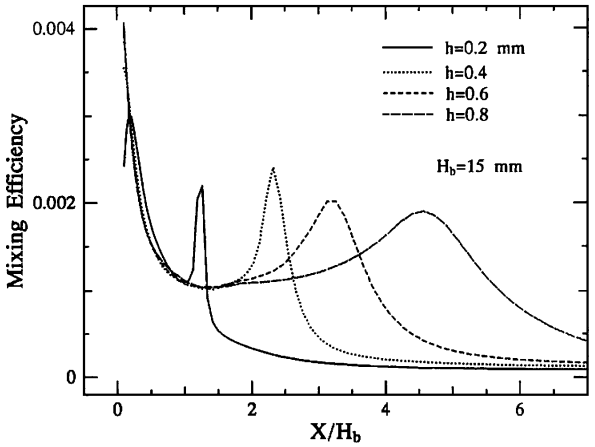

Fig. 8 Variation of mixing efficiency along X, against nozzle exit size h.

resolution in the recirculation region in general and in the injection region in particular is adequately high. Therefore, it can handle a high gradient mixing layer between the jet and the airflow. The velocity profiles and the mixing efficiency variation are shown in Figs. 7 and 8, respectively. The velocity profiles show significant changes in the recirculation region when the size of the nozzle exit increases. The change in the wake flowfield for the small nozzle size ($h = 0.2$ mm) is relatively small compared to the large nozzle ($h = 0.8$ mm). The growth of the mixing regions shown in Fig. 8 is proportional to h and the length of the mixing region. A conclusion based on the data presented in this figure is that the increments of both mixing region length and h are in the same order. For instance, the length of the mixing region at $h = 0.8$ mm reaches to approximately $X/H_b = 6.0$, which is about four times larger than this length at $h = 0.2$ mm. This is concluded from the development of the combustion regions shown in Fig. 9. An effective flame holding is predicted using the numerical results when $h > 4.0$. By increasing h, the substantial combustion region is intensified and expanded with a small shift in downstream direction. However, this can be realized from the variation of the temperature along the centerline as shown Fig. 10.

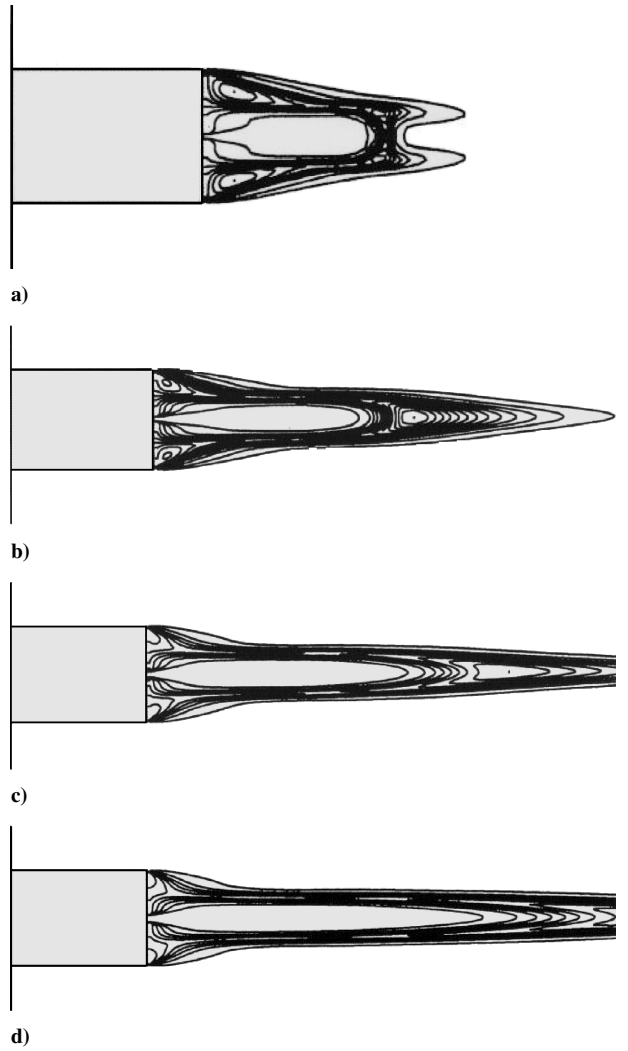

Fig. 9 Distributions of OH mole fraction: a) $h = 0.2$ mm, b) $h = 0.4$ mm, c) $h = 0.6$ mm, and d) $h = 0.8$ mm.

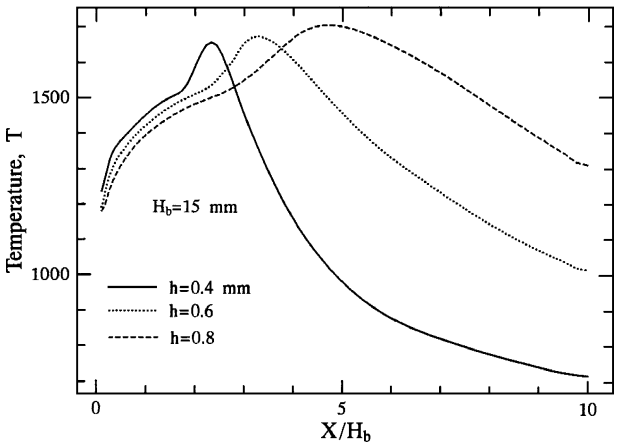

Fig. 10 Variation of temperature along centerline for various h.

Single- and Double-Slit Injection

To investigate the effect of the injection pattern on flame holding, some numerical simulations and experiments were conducted for the single-slit and double-slit injections already shown in Fig. 1. The numerical results on the flowfield and the OH mole fraction profile are shown in Fig. 11. The slit width of the double-slit injection is half of the slit width of the single-slit injection, which provides the same mass flow rate for both settings. The pressure, the density, and especially the velocity at the injection slit also remain the same. The flowfield shown in Fig. 11 represents two different patterns for single-slit and double-slit injections. As it has been already shown for the single-slit injection, the velocity is generally higher near the base because of the fuel injection. Then the fuel flow is decelerated as a result of shear layers. It is again accelerated at the redevelopment region. There is complete reverse flow in the wake providing intense mixing for the double-slit injection. The combustion region is

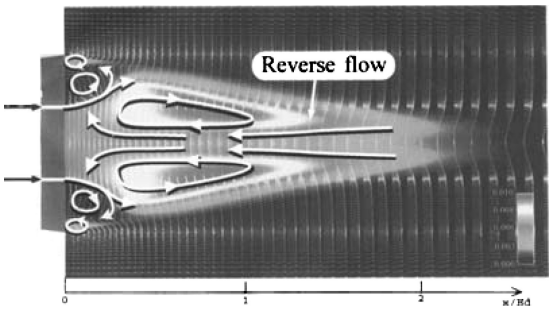

a) Single slit injection ($h = 2$ mm)

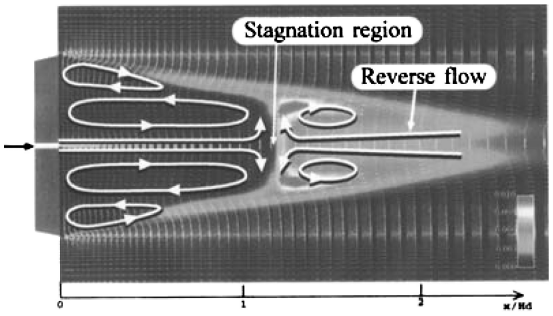

b) Double slit injection ($h = 1$ mm)

Fig. 11 Numerical flowfield and OH distribution.

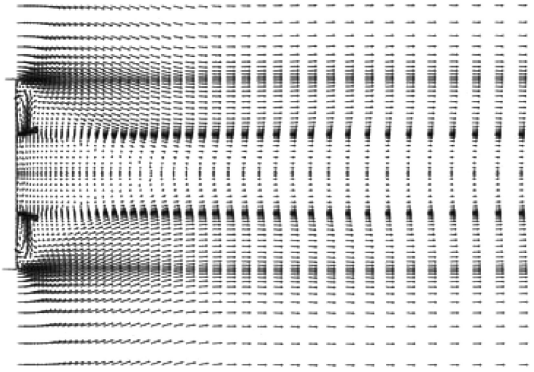

a) $d = 8$ mm

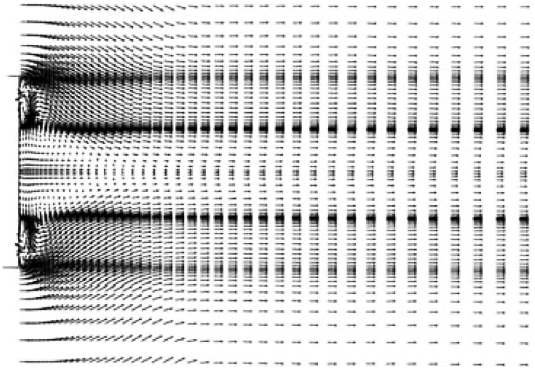

b) $d = 9$ mm

Fig. 12 Velocity flowfield for a) $d = 8$ mm and b) $d = 9$ mm.

demonstrated in Fig. 11 using the OH distribution. For the double-slit injection, a large mixing vortex in the wake is identified near the base.

The distance between two slits, indicated by d, is the slit interval in the double-slit injection. By decreasing the slit interval, the flowfield and the combustion phenomenon move toward the single-slit injection. By increasing the slit interval, the reverse flow region expands laterally, which results in the expansion of the combustion

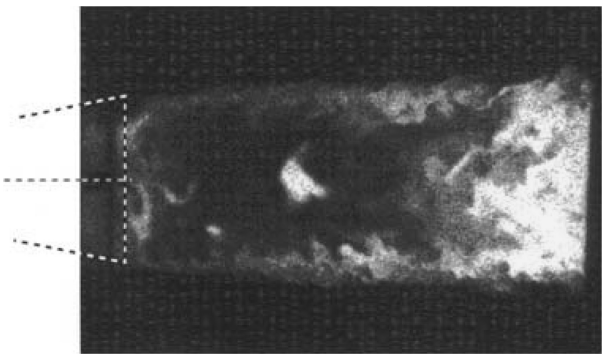

a) Single slit injection ($h = 2$ mm)

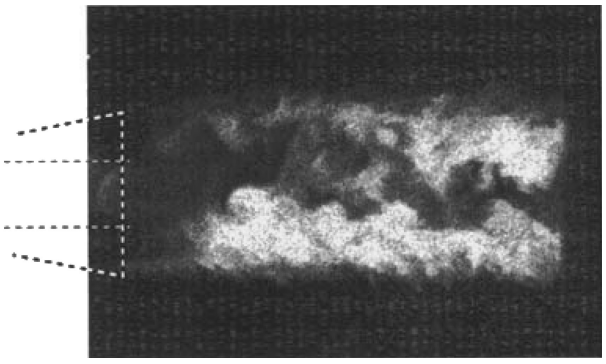

b) Double slit injection ($h = 1$ mm)

Fig. 13 Experimental OH distribution in combustion zone by LIF.

zone. However, the numerical results indicate a flame-holding limit that depends on the slit interval. It seems the flame cannot establish when $d > 8$ mm resulting blowout occurance. Figure 12 shows the reason behind this flame holding and the limited velocity vector field for $d = 8$ and 9 mm, respectively. Figure 12 also demonstrates the fuel jet, which turns into few small recirculation zones close to the corners of the base. Apparently, these small recirculation zones are very essential for the flame holding. The recirculation zone at the corners (i.e., $d = 8$ mm) is large enough to decelerate the main stream airflow. However, the acceleration of the flow at $d = 9$ mm immediately after the corner shows the weakening of the vortex at this location, resulting in no flame holding.

The experiment of the OH-LIF was conducted to investigate the effects of injection modeling on the flame holding. The Nd-YAG laser (GCR-250-10, Spectra Physics) equipped with a dye laser and the ICCD camera (ICCD-576/RB-T, Princeton Instrument, Inc.) is used for the experiments that are conducted for various injection models with different slit intervals. In Fig. 13, the OH-LIF images are shown for two cases of ($d = 0$, $Q_F = 450$ Nl/min) and ($d = 8$ mm, $Q_F = 450$ Nl/min). Comparing with the numerical results of Fig. 11, the experimental OH distributions also confirm the basic flame structure for two aforementioned cases of the injection models. Because of some difficulties to manufacture the experimental model of $d > 8$ mm, the test is limited to the case of $d = 8$ mm. However, the destabilization of the flame at $d = 8$ mm possibly leads blowing out at larger values of the slit interval.

All physical properties of the model are kept constant at the slit exit of the test at $d = 4$ mm, and then the necessary calculations are done by changing parameter h. Figure 14 shows the OH distribution for the cases of $h = 0.2$ and 0.6 mm. Increasing h results in an increase in both the mass flow rate and the jet diameter. This significantly affects the wake flowfield so that the combustion zone is expanding downstream and completely detached from the base. The expansion of the combustion zone downstream in the case of $h = 0.6$ mm is as a result of the large fuel supply.

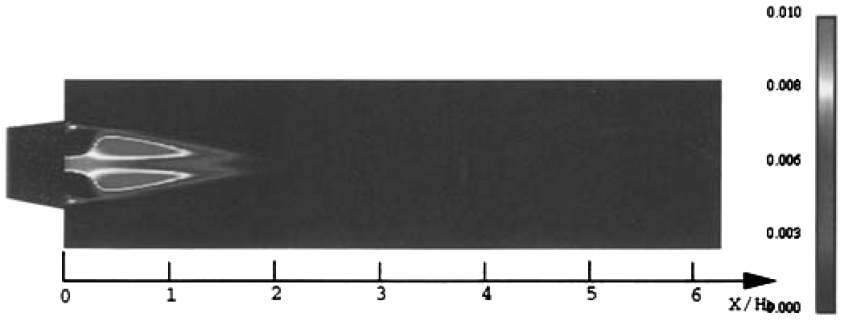

a) $h = 0.2$ mm

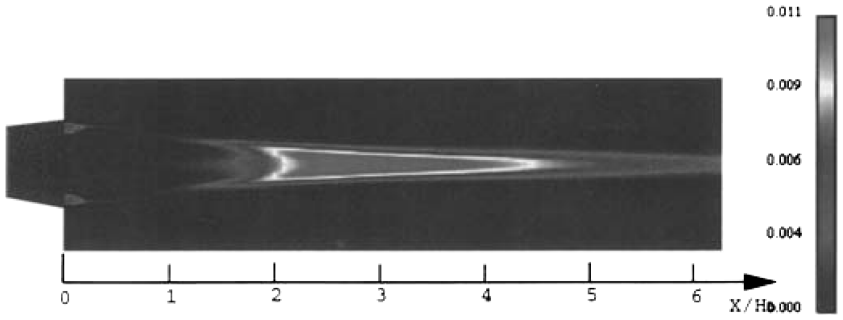

c) $h = 0.6$ mm

Fig. 14 Numerical OH distribution for various slit width h.

Conclusions

In this paper, the results of both numerical and experimental studies on the effect of injection modeling on combustion and flame holding are presented.

The hydrogen fuel is injected from the base of a strut through a single slit or double slit. The flame structure was predicted for two injection models. Two scales that can directly affect recirculation region are the width of the base and the width of the nozzle. Major effects of the variation in these scales are considered on the recirculation region, mixing, and flame holding. It is shown that for the combustion in the supersonic flow similar to what is happening in the subsonic flame the residence time would be directly proportional to the length of the recirculation region. As a result, a wide base can generate a large mixing region causing well-developed combustion zones.

In this paper, both numerical and experimental approaches have been developed to consider the effect of the injections from the single slit or the double slit on the combustion and the flame holding. Changes in the flowfield and the mixing phenomenon can considerably cause the alteration in the flame structure. Increasing the slit interval of the double-slit injection can also blow out when $d > 8$ mm. In addition, an increase of the slit width can considerably affect the wake flowfield so that the combustion zone is expanded downstream.

References

[1]Bogdanoff, D. W., "Advanced Injection and Mixing Techniques for Scramjet Combustors," *Journal of Propulsion and Power*, Vol. 10, No. 2, 1994, pp. 183–190.

[2]Bushnell, D. M., "Hypervelocity Scramjet Mixing Enhancement," *Journal of Propulsion and Power*, Vol. 11, No. 5, 1995, pp. 1088–1090.

[3]Billig, F. S., "Research on Supersonic Combustion," *Journal of Propulsion and Power*, Vol. 9, No. 9, 1993, pp. 499–514.

[4]Kimura, I., Aoki, H., and Kato, M., "The Use of a Plasam Jet for Flame Stabilization and Promotion of Combustion in Supersonic Air Flows," *Combustion and Flame*, Vol. 42, No. 2, 1981, pp. 297–308.

[5]Zukoski, E. E., and Marble, F. E., "Experiment Concerning the Mechanism of Flame Blow-off from Bluff Bodies," *Proceeding of Gas Dynamics Symposium*, Northwestern Univ., Exanston, IL, 1956, pp. 205–210.

[6]Niioka, T., Terada, K., Kobayashi, H., and Hasegawa, S., "Flame Stabilization Characteristics of Strut Divided into Two Parts in Supersonic Airflow," *Journal of Propulsion and Power*, Vol. 11, No. 1, 1995, pp. 112–116.

[7]Chase, M. W., Davies, C. A., Downey, J. R., Frurip, D. J., McDonald, R. A., and Syverud, A. N., *JANNAF Thermochemical Tables*, 3rd ed., Vol. 14, American Inst. of Physics, New York, 1985.

[8]Svehla, R. A., "Estimated Viscosities and Thermal Conductivities of Gases at High Temperature," NASA TR-R-132, June 1962.

[9]Mason, E. A., and Saxena, S. C., "Approximate Formula for the Thermal Conductivity of Gas Mixture," *Physics of Fluids*, Vol. 1, No. 2, 1958, pp. 361–365.

[10]White, F. M., *Viscous Fluid Flow*, McGraw–Hill, New York, 1974.

[11]Wilke, C. R., "A Viscosity Equation for Gas Mixtures," *Journal of Chemical Physics*, Vol. 18, No. 1, 1950, pp. 517–519.

[12]Demetriades, A., and Yapuncich, F. L., "Experimental Tests of a Laminar Mixing Theory," *AIAA Journal*, Vol. 30, No. 7, 1992, pp. 1795–1799.

[13]Pope, S. B., "Computations of Turbulent Combustion: Progress and Challenge," *Proceedings of the 23rd Symposium on Combustion*, Combustion Inst., Pittsburgh, PA, 1990, pp. 591–612.

[14]Bray, K. N. C., Libby, P. A., and Williams, F. A., "High Speed Turbulent Combustion," *Turbulent Reactive Flows*, Academic Press, New York, 1994.

[15]Baurle, R. A., Alexopoulos, E. A., and Hassan, H. A., "Assumed Joint Probability Density Function Approach for Supersonic Turbulent Combustion," *Journal of Propulsion and Power*, Vol. 10, 1994, pp. 473–484.

[16]Coakley, T. J., and Huang, P. G., "Turbulence Modeling for High Speed Flow," AIAA Paper 92-0436, 1992.

[17]Gerlinger, P., Algermissen, J., and Bruggemann, D., "Numerical Simulation of Mixing for Turbulent Slot Injection," *AIAA Journal*, Vol. 34, No. 1, 1996, pp. 73–78.

[18]Stahl, G., and Warnatz, J., "Numerical Investigation of Time-Dependent Properties and Extinction of Strained Methane and Propane Air Flamelets," *Combustion and Flame*, Vol. 85, No. 5, 1991, pp. 285–299.

[19]Shuen, J. S., and Yoon, S., "Numerical Study of Chemically Reacting a Lower-Upper Symmetric Successive Overrelation Scheme," *AIAA Journal*, Vol. 27, No. 12, 1989, pp. 1752–1760.

[20]Ju, Y., "Lower-Upper Scheme for Chemically Reacting Flow with Finite Rate Chemistry," *AIAA Journal*, Vol. 34, No. 8, 1996, pp. 1418–1425.

[21]Gorden, S., and Macbride, B. J., "Computer Program for Calculation of Complex Chemical Equilibrium Compositions, Rocket Performance, Incident and Reflected Shocks, and Chapman–Jouguet Detonations," NASA SP-273, 1971.

[22]Tabejamaat, S., and Niioka, T., "Numerical Study of Preburned Hydrogen by a High-Order Numerical Scheme for Turbulent Reactive Flows," *Proceedings of the Combustion Institute*, Vol. 28, Combustion Inst., Pittsburgh, PA, 2000, pp. 83–89.

[23]Hurina, J. L., and Dutton, J. C., "Two-Stream, Supersonic, Wake Flowfield Behind a Thick Base, Part I: General Features," *AIAA Journal*, Vol. 30, No. 8, 1992, pp. 2039–2046.